Aeroelastic Optimization of a Helicopter Rotor Using an Efficient Sensitivity Analysis

Joon W. Lim* and Inderjit Chopra†
University of Maryland, College Park, Maryland 20742

A structural optimization analysis of a hingeless helicopter rotor is developed and applied with the objective of reducing oscillatory hub loads in forward flight. The aeroelastic analysis of the rotor is based on a finite element method in space and time and is linked with automated optimization algorithms. Two types of structural blade representations are used: a generic stiffness-distribution beam and a single-cell, thin-walled beam. For the generic beam representation the design variables are nonstructural mass and its placement, chordwise center of gravity offset from the elastic axis, and structural stiffness (flap, lag, and torsion). For the second type of structural representation, spar width, height, and thickness are used as design variables instead of blade stiffness. Constraints on frequency placement, autorotational inertia, and aeroelastic stability of the blade are included. Sensitivity derivatives are efficiently calculated using a direct analytical approach, with a resulting 80% reduction in total CPU time required to obtain an optimum solution compared with a commonly used finite-difference approach. Optimum solutions resulted in reductions of 25–77% for the generic blade, and 30–50% for the box-beam blade relative to baseline values of the objective function that was comprised of all six components of hub load.

Nomenclature

c = blade chord
$\boldsymbol{D}$ = design variables D_j, $J = 1,...,n$
e_d = chordwise offset of aerodynamic center from the elastic axis (positive forward)
e_g = effective chordwise offset of blade c.g. from the elastic axis (positive forward).
EA = blade extensional stiffness
EI_y = blade flap bending stiffness
EI_z = blade lag bending stiffness
GJ = blade torsional stiffness
$\boldsymbol{K}_t$ = tangential stiffness matrix
m = number of blade normal modes
m_{ns} = nonstructural mass per unit length
m_0 = reference mass per unit length
N = number of beam elements
N_b = number of blades
n = number of design values
$\boldsymbol{Q}$ = state variables of load vectors
$\boldsymbol{q}$ = blade global coordinates
$\boldsymbol{T}_c$ = coordinate transformation matrix
$\boldsymbol{X}$ = state variables of blade nodal response for time elements
y_{ns} = chordwise offset of nonstructural mass from the elastic axis (positive forward)
y_0 = chordwise offset of baseline blade c.g. from the elastic axis (positive forward)
α_k = real part of characteristic exponent of kth mode
λ_k = eigenvalue of kth mode
$\boldsymbol{\Phi}$ = transition matrix of perturbation equations
ψ = azimuth angle
ω_k = blade natural frequency of kth mode

Subscripts

H = hub-fixed nonrotating frame
R = rotating (undeformed blade) frame

Superscripts

P = per rev
0 = baseline blade configuration

Received Jan. 20, 1990; revision received April 26, 1990; accepted for publication April 27, 1990.

*Research Associate, Center for Rotorcraft Education and Research, Department of Aerospace Engineering; currently Professional Staff, Sterling Federal Systems, Moffett Field, CA.

†Professor, Center for Rotorcraft Education and Research, Department of Aerospace Engineering. Associate Fellow AIAA.

Introduction

STRUCTURAL optimization with aeroelastic constraints has received considerable attention in the fixed-wing field.[1] Recently, there have been increasing efforts to apply structural optimization to rotary-wing problems. The potential of structural optimization is further enhanced by the application of composites in blade construction, which permits great flexibility in tailoring structural characteristics. Also, with the availability of refined optimization algorithms and the substantially increased processing capability of computers, it is becoming more attractive to implement aeroelastic optimization in the design of complex rotor systems.

Recently, there have been some attempts to explore aeroelastic optimization of a rotor system for vibration reduction. Friedmann and Shanthakumaran[2] applied a modern structural optimization procedure using a sequential unconstrained minimization technique[3] (SUMT) to reduce oscillatory hub loads (thrust or rolling moment) for a four-bladed hingeless rotor by redistributing the mass and stiffness properties of the rotor blades. They imposed constraints on rotating frequencies and aeroelastic stability in hover. Peters et al.[4] applied the method of feasible directions[5] (CONMIN) to optimize the placement of blade rotating frequencies and minimize rotor weight by modifying the dimensions of a box-beam blade. A rotor aeroelastic analysis was not used in this study. Bennett[6] used the generalized reduced gradient approach (OPT[7]) to optimize rotor design parameters in solving several sample problems: minimizing blade stress, vertical shear, rotor mast weight, and power requirement in hover. Davis and Weller[8] applied an automated design synthesis code (ADS[9]) to solve four different rotor design problems: maximizing bearingless rotor in-plane damping, placing blade natural frequencies, minimizing hub modal shears, and minimizing rotor modal vibration indices. Aeroelastic stability constraints were not considered in the optimization process. Most of these works did not concentrate on the computational efficiency of evaluating the sensitivity derivatives for the optimization procedure but did show the potential of aeroelastic optimization in rotorcraft.

One of the key considerations in developing an efficient optimization analysis is to minimize computations devoted to calculating sensitivity derivatives of objective and constraint functions with respect to different design variables. This is especially important for the computationally expensive problem of aeroelastic optimization of a helicopter rotor. Most previous rotor optimization studies used finite-difference approaches to calculate sensitivity derivatives. Therefore, much larger computation times were needed to obtain optimum solutions than if sensitivity derivatives could have been calculated analytically. Lim and Chopra[10,11] addressed this issue by deriving efficient analytical sensitivity formulations for hub loads and blade stability and incorporating them as integral parts of aeroelastic response and stability analyses. The authors coupled the analysis with CONMIN[5] and carried out a comprehensive optimization study[12] to reduce vibrations in a helicopter with a four-bladed hingeless rotor. It was shown that a substantial reduction of CPU time could be achieved in the optimization procedure, compared to commonly used finite-difference approaches. Also, Celi and Friedmann[13] constructed a sequence of approximate optimization problems[14] for an efficient sensitivity analysis and then minimized the oscillatory vertical hub shear for a hingeless rotor with both straight and swept tip blades. They imposed constraints on frequency, autorotation, and blade stability in hover, and showed a large reduction of the number of function evaluations in the optimization procedure, compared to finite-difference approaches. Chattopadhyay and Walsh[15] applied an approximate reanalysis technique[16] to calculate sensitivity derivatives of frequency constraints. Also, Pritchard and Adelman[17] obtained the derivatives of a modal shaping parameter by a hybrid sensitivity analysis using Nelson's method[18] for eigenvector derivatives and finite differences for mass matrix derivatives. All these recent efforts were directed to obtain efficient sensitivity derivatives for aeroelastic optimization of rotors.

The objective of this study is to perform an aeroelastic optimization of a helicopter rotor using efficient sensitivity analyses and to examine the influence of the behavior constraints in the optimization procedure. An automated optimization procedure is developed by coupling the rotor dynamics analysis and design sensitivity analysis with a constrained optimization program CONMIN.[5] The rotor dynamics analysis is based on a finite element method in space and time.[19] The design sensitivity analysis uses a direct analytical approach.[10,11] To reduce helicopter vibrations, the objective function included all six components of 4P hub loads for a four-bladed hingeless rotor, while maintaining constraints on aeroelastic stability, frequency placement, and autorotational inertia. Optimum solutions are obtained for two types of blade structural representations. One is a generic rotor blade whose structural properties are described in terms of blade stiffnesses, regardless of the cross-sectional details. In the second type, the blade structural characteristics are defined in terms of a spar geometry of a closed-cell box beam.

Rotor Dynamics Analysis

The rotor dynamic analysis used in the present study was developed at the University of Maryland and is based on a finite element method in space and time.[19,20] This analysis consists of two major phases: coupled vehicle trim with rotor steady response and aeroelastic blade stability. Each blade is assumed to be an elastic beam undergoing flap bending, lag bending, elastic twist, and axial deflections. The analysis is developed for a nonuniform blade having pretwist and precone, as well as chordwise offsets of blade center of gravity, aerodynamic center, and tensile axis from the elastic axis.

The blade steady response solution involves determination of time-dependent blade deflections at different azimuth locations. To reduce computation time, the finite element equations are transformed to the normal mode domain using the coupled natural vibration modes of the blade. These nonlinear periodic equations are then solved using a finite element method in time. The hub loads are obtained using a force summation method. For this, the motion-induced aerodynamic and inertial loads are integrated along the blade span to obtain the blade loads at the root and are then summed over all the blades to obtain the rotor hub loads.

The trim solution is calculated from the overall nonlinear vehicle equilibrium equations. For the coupled trim analysis, the vehicle trim and rotor response equations are solved iteratively as one coupled solution using a modified Newton method. As a result, the converged solution satisfies simultaneously the overall vehicle force and moment equilibrium equations, as well as the nonlinear blade equations of motion.

For the stability analysis, the blade perturbation equations of motion are linearized about the equilibrium position and are then transformed to the normal mode domain. The normal mode equations contain periodic terms, and these equations are solved for complex eigenvalues using Floquet transition matrix theory. Blade damping is obtained from the complex eigenvalues.

Optimization Analysis

Mathematically, the optimization problem can be described in the following form:

Minimize: $J(\boldsymbol{D})$ (objective function)

Subject to: $\boldsymbol{g}(\boldsymbol{D}) \leq 0$ (inequality constraints)

$$\boldsymbol{D}^L \leq \boldsymbol{D} \leq \boldsymbol{D}^U \text{ (side constraints)}$$

where $\boldsymbol{D}$ are design variables and superscripts L and U denote lower and upper bounds. For the study described herein, the objective function includes oscillatory hub loads to reduce vibrations, while inequality constraints are maintained on aeroelastic stability, frequency placement, and autorotational inertia. The design variables are bounded by the side constraints. For a feasible design, the solution must lie within the design space bounded by inequality and side constraints.

Design Variables

In order to obtain an optimum solution for the vibration reduction of a helicopter, one needs to consider several blade design parameters. For the generic blade representation, the design variables are nonstructural mass and its chordwise placement, chordwise center of gravity offset, and structural stiffnesses (flap, lag, and torsion). It consists of six design variables per spanwise blade element. For a box-beam representation, dimensions of the spar are used as design variables instead of blade stiffnesses. Hence, the design variables are nonstructural mass and its chordwise placement, chordwise center of gravity offset, and width, height, and thicknesses of the spar. Thus, seven design variables per element are required.

Behavior Constraints

The present optimization study includes three frequently used behavior constraints: 1) aeroelastic stability, 2) frequency placement, and 3) autorotational inertia. The aeroelastic stability constraint is needed to keep the rotor blades stable in flight. Blade stability in forward flight is calculated using Floquet theory. The stability constraint is expressed as

$$g_{S_k}(\boldsymbol{D}) = \alpha_k + \varepsilon_k \leq 0, \qquad k = 1,...,m \tag{1}$$

where ε_k (positive number) is the minimum allowable blade damping for the kth mode, and the real part of the stability root α_k is defined as

$$\alpha_k = (1/T)\ell n \sqrt{(\lambda_k^R)^2 + (\lambda_k^I)^2} \tag{2}$$

The symbol T is one period of rotor revolution (i.e., 2π), λ is the eigenvalue of the Floquet transition matrix, and the superscripts R and I denote real and imaginary parts, respectively. The details for the stability analysis are available in Ref. 11. It may be noted that a negative value of α_k represents a positive damping of the kth mode.

The frequency placement constraints ensure that the blade rotating frequencies occur within desired ranges to avoid blade resonance at frequencies not covered by the objective function and to maintain acceptable fundamental frequencies. The frequency constraint can be written as

Lower bound:

$$g^L_{F_k}(\boldsymbol{D}) = 1 - \omega_k/\omega^L_k \le 0, \quad k = 1,...,m \tag{3}$$

Upper bound:

$$g^U_{F_k}(\boldsymbol{D}) = \omega_k/\omega^U_k - 1 \le 0, \quad k = 1,...,m \tag{4}$$

where ω_k is the blade rotating frequency for the kth mode and superscripts L and U denote the lower and upper bounds, respectively. Note that the blade rotating frequencies are obtained from a coupled free vibration analysis:

$$(\boldsymbol{K}^s - \omega^2_k \boldsymbol{M}^s)\boldsymbol{\phi} = 0 \tag{5}$$

where superscript s denotes the structural part and K and M are stiffness and mass matrices of the rotor blade. The symbol $\boldsymbol{\phi}$ is the corresponding eigenmode.

Finally, the autorotation constraint implies that a rotor must have sufficient inertia for a safe autorotation.

$$g_A(\boldsymbol{D}) = R_A - \frac{I}{I_b} = R_A - \sum_{i=1}^{N} m_i(x^3_{i-1} - x^3_i) \le 0 \tag{6}$$

where m_i is blade mass per unit length of the ith spanwise beam element, nondimensionalized by the reference mass, and x_i is a distance of the left end of the ith beam element from the blade root divided by the rotor radius. The symbol R_A is the minimum allowable value of the ratio of the blade moment of inertia I to the baseline value I_b.

Design Sensitivity Analysis

The objective function and constraints are expressed in terms of blade response and design variables. The blade response, however, also depends on the design variables. Therefore, the sensitivity derivatives of the objective function and constaints, with respect to design variables, are obtained by chain rule differentiation in the following form:

$$\frac{dF}{dD_j} = \frac{\partial F}{\partial D_j} + \frac{\partial F}{\partial \boldsymbol{Y}}\frac{\partial \boldsymbol{Y}}{\partial D_j}, \qquad j = 1,...,n \tag{7}$$

where $\boldsymbol{Y}$ is the blade response.

The design sensitivity analysis, which an optimizer requires, is carried out by calculating gradients of steady response, hub loads, blade stability, blade frequencies, and autorotational inertia.

Response Sensitivity Analysis

The formulation of sensitivity derivatives of blade response is developed as an integral part of the basic steady response analysis. Using a finite element approach in time, the blade response is derived from the virtual energy expression (Hamilton's principle in weak form). For the derivatives of the blade response, the virtual energy is differentiated with respect to the design variables using a direct analytical approach and would result in the following expression:

$$\frac{\partial \boldsymbol{X}^G}{\partial D_j} = -(\boldsymbol{K}^G_t)^{-1}\frac{\partial \boldsymbol{Q}^G}{\partial D_j} \tag{8}$$

where

$$\boldsymbol{K}_t = \begin{bmatrix} \dfrac{\partial \boldsymbol{F}}{\partial \boldsymbol{q}} - \boldsymbol{K} & \dfrac{\partial \boldsymbol{F}}{\partial \dot{\boldsymbol{q}}} - \boldsymbol{C} \\ \boldsymbol{0} & \boldsymbol{M} \end{bmatrix}$$

$$\boldsymbol{Q} = \begin{Bmatrix} \boldsymbol{F} - \boldsymbol{C}\dot{\boldsymbol{q}} - \boldsymbol{K}\boldsymbol{q} \\ \boldsymbol{M}\dot{\boldsymbol{q}} \end{Bmatrix}$$

and where $\boldsymbol{q}$ is the blade steady response, and $\boldsymbol{M}$, $\boldsymbol{C}$, $\boldsymbol{K}$, and $\boldsymbol{F}$ are mass, damping, and stiffness matrices and force vector, respectively, and $\boldsymbol{X}$ is a state variable for the nodal response in a time element. The global matrices are referred by the superscript G and are obtained by assembling the time elements for one complete revolution. The calculation of the global tangential matrix $\boldsymbol{K}^G_t$ is a part of the steady response solution and is used here to calculate response derivatives. The details for this part are presented in Ref. 10.

Hub Loads Sensitivity Analysis

Using a force summation approach, the blade root loads are calculated by summing the aerodynamic and inertial loads along the blade; these are expressed explicitly in terms of design variables as well as blade response. The hub loads are obtained by transforming blade root loads into the hub-fixed nonrotating frame and then summing these for all blades. The derivatives of the loads are obtained as

$$\frac{d\boldsymbol{F}_H}{dD_j} = \sum_{n=1}^{N_b} \boldsymbol{T}^T_C \frac{d\boldsymbol{F}^{(n)}_R}{dD_j} \tag{9a}$$

$$\frac{d\boldsymbol{M}_H}{dD_j} = \sum_{n=1}^{N_b} \boldsymbol{T}^T_C \frac{d\boldsymbol{M}^{(n)}_R}{dD_j} \tag{9b}$$

where subscripts R and H represent rotating frame and fixed system nonrotating hub frame, respectively, and N_b is the number of blades. The matrix $\boldsymbol{T}_c$ is a transformation matrix from the rotating to the nonrotating frame and is defined in Ref. 21.

Stability Sensitivity Analysis

The stability sensitivity analysis involves differentiation of the eigenvalues for the aeroelastic stability of the rotor blades and is calculated as an integral part of the basic stability analysis. The derivatives of the kth eigenvalue are given in terms of the derivatives of the transition matrix obtained using Floquet theory[11]

$$\frac{d\lambda_k}{dD_j} = \frac{d\lambda^R_k}{dD_j} + i\frac{d\lambda^I_k}{dD_j}$$

$$= \boldsymbol{y}^T \frac{d\boldsymbol{\Phi}(\psi_0 + T, \psi_0)}{dD_j}\boldsymbol{x} \tag{10}$$

where $\boldsymbol{x}$ is the normalized complex eigenvector and $\boldsymbol{y}$ is the corresponding left eigenvector, such that $\boldsymbol{y}^T\boldsymbol{x} = 1$. The sensitivity derivatives of the stability constraints are defined as

$$\frac{dg_{S_k}}{dD_j} = \frac{d\alpha_k}{dD_j}, \qquad k = 1,...,m \tag{11}$$

From Eq. (2), the derivatives of the real part of stability roots are calculated as

$$\frac{d\alpha_k}{dD_j} = \frac{1}{T} - \frac{\lambda^R_k \dfrac{d\lambda^R_k}{dD_j} + \lambda^I_k \dfrac{d\lambda^I_k}{dD_j}}{(\lambda^R_k)^2 + (\lambda^I_k)^2} \tag{12}$$

Frequency Sensitivity Analysis

The sensitivity derivatives of blade rotating frequencies are formulated from the eigenanalysis of free vibrations of the blade. Differentiating Eq. (5) with respect to D_j, one obtains

$$(2\omega_k \boldsymbol{M}^s\boldsymbol{\phi})\frac{d\omega_k}{dD_j} = \left(\frac{d\boldsymbol{K}^s}{dD_j} - \omega_k^2\frac{d\boldsymbol{M}^s}{dD_j}\right)\boldsymbol{\phi} + (\boldsymbol{K}^s - \omega_k^2\boldsymbol{M}^s)\frac{d\boldsymbol{\phi}}{dD_j} \tag{13}$$

The second term in the right side is dropped due to Eq. (5) and then premultiplying by the eigenvector $\boldsymbol{\phi}^T$ results in the following expression:

$$(2\omega_k \boldsymbol{m}^s)\frac{d\omega_k}{dD_j} = \frac{d\boldsymbol{k}^s}{dD_j} - \omega_k^2\frac{d\boldsymbol{m}^s}{dD_j} \tag{14}$$

where the matrices $\boldsymbol{m}^s$ and $\boldsymbol{k}^s$ are the generalized mass and stiffness matrices, respectively: $\boldsymbol{m}^s = \boldsymbol{\phi}^T\boldsymbol{M}^s\boldsymbol{\phi}$ and $\boldsymbol{k}^s = \boldsymbol{\phi}^T\boldsymbol{K}\boldsymbol{\phi}$.

Equation (14) can be solved for the derivatives of the frequency using standard linear equation solvers. The sensitivity derivatives of frequency constraints, which are linear functions of frequency, are readily obtained using Eq. (7).

Autorotation Sensitivity Analysis

The formulation of the derivatives of autorotation constraint is straightforward and is derived by differentiating the autorotation inertia with respect to the design variables and using Eq. (7):

$$\frac{dg_A}{dD_j} = \begin{cases} -(x_{i-1}^3 - x_i^3), & D_j = m_{ns}^i \\ -\dfrac{\rho_s}{E}(x_{i-1}^3 - x_i^3), & D_j = EA_s^i \\ 0 & \text{otherwise} \end{cases} \tag{15}$$

where ρ_s is mass density, E is a Young's modulus of the structural part of the rotor blade, and superscript i denotes ith beam element.

Single-Spar Blade

The blade consists of a single spar and is represented by a box beam, as shown in Fig. 1. The box beam has a width of b_s, height of h_s, and thicknesses t_b and t_h. The portion of blade structural stiffness due to the box beam can be derived to give

$$EI_y = \int\int E\zeta^2\,d\eta\,d\zeta = \frac{Eh_s^2}{6}(3b_st_b + h_st_h) \tag{16a}$$

$$EI_z = \int\int E\eta^2\,d\eta\,d\zeta = \frac{Eb_s^2}{6}(b_st_b + 3h_st_h) \tag{16b}$$

$$GJ \approx G\frac{2b_s^2h_s^2t_bt_h}{(b_st_h + h_st_b)} \tag{16c}$$

$$EA_s \approx 2E(b_st_b + h_st_h) \tag{16d}$$

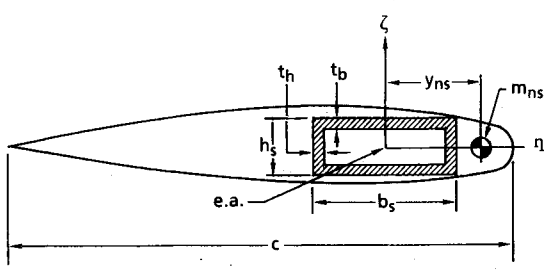

Fig. 1 Blade cross section with a box beam.

Table 1 Baseline hingeless blade structural properties

$EI_y/m_0\Omega^2R^4$	0.01080
$EI_z/m_0\Omega^2R^4$	0.02680
$GJ/m_0\Omega^2R^4$	0.00615
k_A/R	0.0290
k_{m1}/R	0.0132
k_{m2}/R	0.0247

Note that the torsional constant J for the thin-walled closed section is calculated using Bredt's formula[22]:

$$J = 4(\text{section area})^2 \Big/ \oint(ds/\text{thickness}) \tag{17}$$

The baseline blade is considered to have structural mass as well as a certain amount of nonstructural mass. The structural mass area is given as

$$m_s \approx 2(b_st_b + h_st_h) \tag{18}$$

The baseline nonstructural mass is contributed from the leading-edge lumped mass, honeycomb, skin, etc. The resulting blade mass is defined as a sum of the masses of the structural and nonstructural parts, such that

$$m = m_s + m_{ns}^0 + m_{ns} \tag{19}$$

where m_{ns}^0 is the invariant baseline nonstructural mass and m_{ns} is additional nonstructural mass used by the optimizer as a design variable. Variation in the dimensions of the box beam, such as the width, height, and thicknesses, would change the blade mass as well as the blade stiffnesses.

The design variables for the box-beam blade are the dimensions of the box beam (b_s,h_s,t_b,t_h) and the nonstructural design parameters (m_{ns},y_{ns},y_0). The generic structural design variables $\boldsymbol{D}$, which include EI_y,EI_z,GJ,EA_s, are expressed as a function of new blade design variables B_j, which are b_s,h_s,t_b,t_h. This means that

$$\boldsymbol{D} = \boldsymbol{D}(B_j) \tag{20}$$

Therefore, one would describe the sensitivity derivatives with B_j as follows:

$$\frac{dJ}{dB_j} = \frac{dJ}{d\boldsymbol{D}}\frac{\partial \boldsymbol{D}}{\partial B_j} \tag{21}$$

Results and Discussion

Numerical results are calculated for a four-bladed soft in-plane hingeless rotor with Lock number $\gamma = 5.5$, solidity ratio $\sigma = 0.07$, thrust level $c_W/\sigma = 0.07$, blade aspect ratio $c/R = 0.055$, zero precone and zero pretwist. The chordwise center of gravity offset, aerodynamic center, and tensile axis from the elastic axis (y_0, e_d, and e_A) are assumed to be zero for the baseline configuration. The elastic axis is assumed to be located at quarter-chord. The fuselage center of gravity lies on the shaft axis ($X_{CG} = Y_{CG} = 0$) and is located at a distance of $0.2R$ below the rotor hub center. The fuselage drag coefficient in terms of flat plate area, i.e., $f/\pi R^2$ is taken as 0.01. The airfoil characteristics used are $c_l = 2\pi\alpha$, $c_d = 0.01$, and $c_m = 0.0$.

For the analysis, the blade is discretized into five spanwise beam elements of equal length, and each element consists of 15 nodal degrees of freedom. For the calculation of blade steady response, eight coupled rotating natural modes (2 flap, 2 lag, 2 torsion, and 2 axial modes) are used. For the periodic steady response of the rotor, one period of rotor revolution is discretized into six time elements, and each time element is described by a quartic Lagrange polynomial distribution

along the azimuth. For the stability calculation, 2 flap, 2 lag, and 2 torsion modes are used; the axial modes do not appear to have an important influence on blade stability. The modes are obtained about the mean deflected position of the blade. This modeling approximation yields satisfactory converged results.

Optimization of Generic Blade

For the baseline blade configuration, the rotating natural frequencies are 1.13/rev for the flap, 0.70/rev for the lag, and 4.47/rev for the torsion modes. These structural properties are given in Table 1.

In the iterative optimization procedure, a major part of total CPU time is used to calculate senstivity derivatives. Figure 2 shows the efficiency of the present sensitivity analysis (direct analytical approach) compared with a commonly used finite-difference approach. For numerical calculations, the UNISYS-1100/90 mainframe computer is used. This sensitivity analysis includes the calculation of sensitivity derivatives of blade response, oscillatory hub loads (objective function), and damping (behavior constraint) of the baseline blade. Typically, for a case involving five design variables, the required CPU time is 110 min for the finite-difference approach and 25 min for the direct analytical approach. For 30 design variables, the CPU time is increased to 560 min for the finite-difference approach, whereas the analytical approach takes 50 min. As the number of design variables increases, the use of the direct analytical approach results in dramatic increases in efficiency compared to the finite-difference approach.

In the optimization analysis, design variables are controlled by side constraints. The upper and lower bounds for the side constraints are chosen so as to produce a sufficiently large but variable design space. These bounds are given for each beam element as follows.

Nonstructural mass:

$$0 \le (m_{ns}/m_0) \le 0.25$$

Nonstructural mass c.g.:

$$-0.20 \le (y_{ns}/c) \le 0.20$$

Blade c.g. offset:

$$-0.10 \le (y_0/c) \le 0.10$$

Flap bending stiffness:

$$0.50 \le (EI_y/EI_y^0) \le 1.50$$

Lag bending stiffness:

$$0.50 \le (EI_z/EI_z^0) \le 1.50$$

Torsion stiffness:

$$0.50 \le (GJ/GJ^0) \le 1.50$$

For the initial design, a small nonstructural mass of 1% of the baseline blade mass per unit length is added to the baseline blade, placed uniformly along the blade span at a chord location of $0.05c$ (5% of chord) forward from the elastic axis (toward the leading edge). It is assumed that the structural mass of the blade is fixed and, thus, the blade axial stiffness EA_s is unchanged. In the optimization process, the scale factors for the optimization code CONMIN are determined through a sensitivity analysis; they are 1.0 for m_{ns}, 0.2 for y_{ns}, 0.1 for y_0, and 0.01 for blade bending stiffnesses (EI_y, EI_z, and GJ). For convenience, the frequency and autorotation constraints are not imposed in the optimization analysis for this case. The aeroelastic stability constraints are retained, such that the first lap, lag, and torsion modes remain stable.

For helicopter vibration reduction, it is common to define the objective function to include oscillatory hub loads, which consist of three components of hub forces and three components of hub moments. For a fully articulated rotor with N_b blades, N_b/rev vertical root shear is transmitted to the hub and no blade moment is transmitted to the hub. With a hinge offset, N_b/rev vertical root shear is transmitted to the hub and $(N_b \pm 1)$/rev vertical root shears are transmitted in the form of hub moments. For advanced rotors such as hingeless and bearingless rotors, the oscillatory blade root moments as well as root shears are transmitted to the hub and these affect the vibration in the airframe. Therefore, the objective function for vibration reduction should include the contributions from all significant components of oscillatory hub forces and moments. In the present analysis, the objective function is defined as a sum of 4/rev hub force resultant and 4/rev hub moment resultant.[13] The weighting functions for both force and moment resultants are chosen as unity. In nondimensional form, the objective function becomes

$$J = \sqrt{(\bar{F}_{XH}^{4P})^2 + (\bar{F}_{YH}^{4P})^2 + (\bar{F}_{ZH}^{4P})^2} + \sqrt{(\bar{M}_{XH}^{4P})^2 + (\bar{M}_{YH}^{4P})^2 + \bar{M}_{ZH}^{4P})^2} \qquad (22)$$

The hub forces and moments are nondimensionalized with respect to $m_0\Omega^2R^2$ and $m_0\Omega^2R^3$, respectively. In order to achieve an optimum solution, the best choice of design variables, as determined in Ref. 13, is nonstructural masses and their locations (chordwise) and the spanwise distribution of blade flap bending, lag bending, and torsional stiffnesses. In this case, for five beam elements, 25 design variables were used. Figure 3 shows the optimization iteration history of the objective function. Each iteration involves updating the search direction based on results of the sensitivity analysis, determining the optimum move in a one-dimensional search,

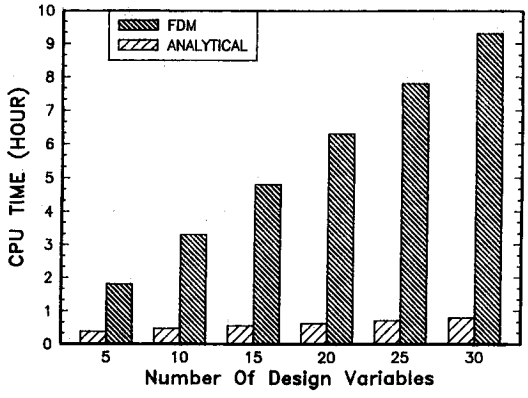

Fig. 2 Comparison of CPU time for design sensitivity analysis.

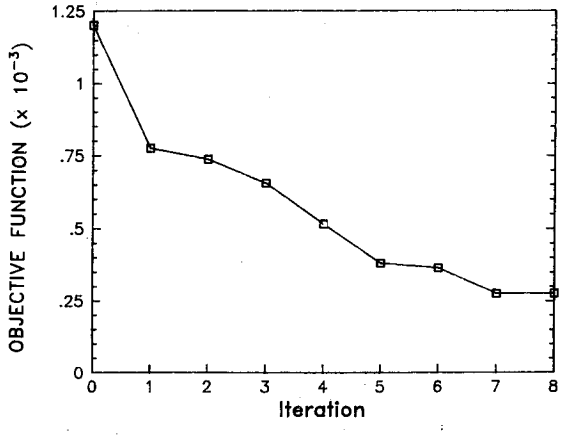

Fig. 3 Optimization iteration history of objective function.

and checking for convergence to terminate the optimization process. The termination criteria for the optimum solution is chosen such that either the relative change in the objective function $<0.1\%$ or the absolute change $<10^{-6}$ between subsequent iteration steps. For the behavior constraints, the aeroelastic stability of the blade is imposed. For this, a minimum allowable damping for the blade stability is taken to be zero. The optimum solution is obtained after eight iterations, and a 77% reduction of the objective function is achieved.

Figure 4 compares the resulting 4/rev hub forces and moments with baseline values. All 4/rev hub forces and moments are shown to be significantly smaller than the baseline values: an 80% reduction for longitudinal and lateral hub shears, a 60% reduction for vertical hub shears, and 80% reduction for rolling and pitching hub moments, and a 90% reduction for yawing hub moment.

Figure 5 shows a comparison of CPU time for the complete optimization solution using finite-difference and direct analytical approach. For the finite-difference approach, the CPU time is estimated based on the number of function evaluations required using the direct analytical approach. To achieve an optimum solution, there is about an 80% reduction in CPU time with a direct analytical approach, compared to the commonly used finite-difference approach. The substantial reduction of CPU time in the optimization procedure is a result of the efficient evaluation of sensitivity derivatives of the objective and constraint functions using a direct analytical approach.

Table 2 Baseline box-beam blade parameters

$b_s = 3.0$ in.
$h_s = 1.2$ in.
$t_b = 0.3$ in.
$t_h = 0.3$ in.
$E = 10.5\ (\times 10^6$ psi)
$G = 2.6\ (\times 10^6$ psi)
$\rho g = 0.08$ lb/in.
$\Omega = 360$ rpm
$R = 193$ in.
$c = 10.6$ in.

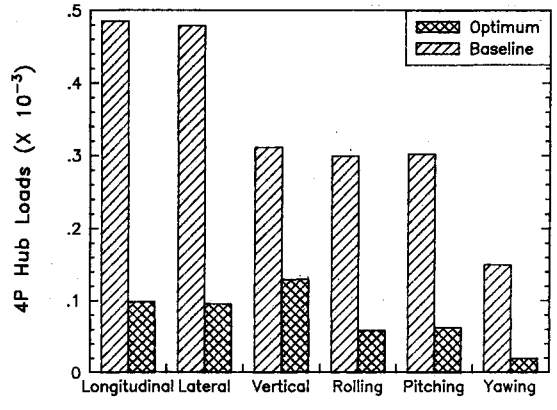

Fig. 4 Optimum 4/rev hub forces and moments.

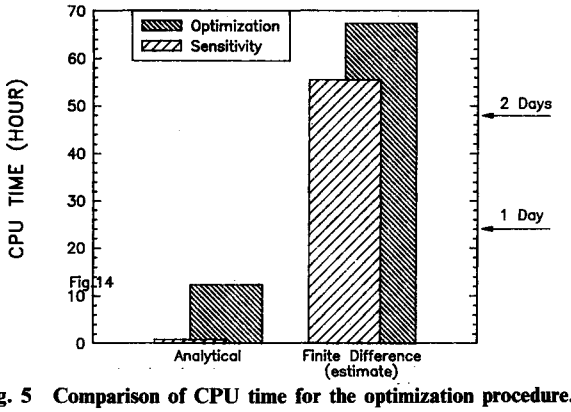

Fig. 5 Comparison of CPU time for the optimization procedure.

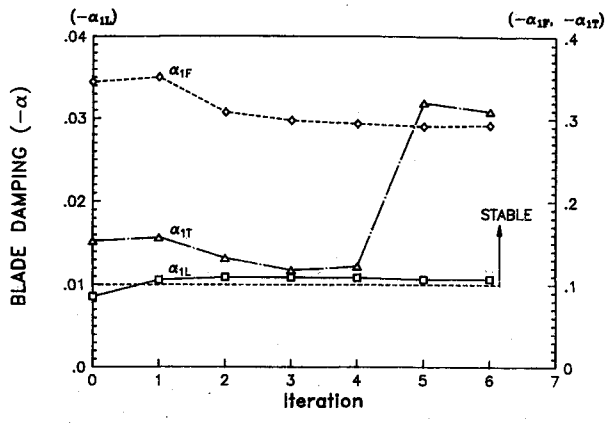

Fig. 6 Optimization iteration history of blade damping, initially infeasible.

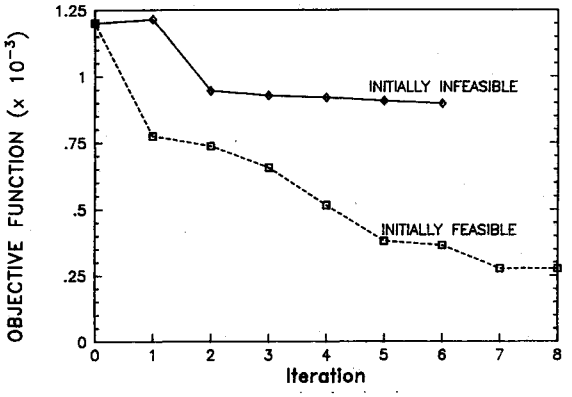

Fig. 7 Optimization iteration history of objective function, initially infeasible and feasible.

For the case shown in Fig. 3, the aeroelastic stability constraint never became active. For the aeroelastic stability constraint to become active in the optimization process, a margin of 1% for blade damping is imposed. This condition turns the baseline design into an initially infeasible design. Figure 6 shows the optimization iteration history of the stability constraint for this design. For stability, the blade damping of the first lag, flap, and torsion modes are considered. The lag mode damping is initially $<1\%$, which violates the stability constraint. After one iteration, the design solution is moved into the feasible design space along the feasible direction by the optimizer CONMIN,[5] and the blade becomes aeroelastically stable. In subsequent iterations, blade stability is well maintained. Note that the blade damping of the lag and flap modes varies smoothly at each iteration, but that the torsion mode damping changes abruptly between the fourth and fifth iterations. This is a result of a large shift of effective center of gravity caused by the placement of nonstructural mass.

Figure 7 shows the optimization iteration history of the objective function for the case where the aeroelastic stability constraint is violated by the initial design (initially infeasible). For comparison, the initially feasible case of Fig. 3 is also shown. During the first iteration, the optimizer changes the design solution until the first lag mode damping is no longer violated. The design solution becomes feasible, and the objective function is slightly increased. In subsequent iterations, the objective function is continuously reduced. The optimum solution for the initially infeasible design case is obtained after six iterations, resulting in a 25% reduction in the objective

Table 3 Iteration history of behavior constraints for case 1 (no behavior constraint imposed)

	Iteration									
	0	1	2	3	4	5	6	7	8	9
ω_{1L}/rev	0.7290	0.7190	0.6710	0.6540	0.6070	0.6000	0.5940	0.5730	0.5350	0.5350
ω_{1F}/rev	1.101	1.099	1.089	1.086	1.078	1.075	1.073	1.067	1.061	1.061
ω_{1T}/rev	4.251	4.203	3.993	3.919	3.741	3.693	3.650	3.502	3.284	3.284
I/I_b	1.010	0.992	0.966	0.963	0.959	0.955	0.958	0.965	0.978	0.078
α_{1L}	−0.0221	−0.0227	−0.0218	−0.0213	−0.0179	−0.0175	−0.0173	−0.0163	−0.0158	−0.0158
α_{1F}	−0.3274	−0.3347	−0.3495	−0.3519	−0.3458	−0.3431	−0.3410	−0.3334	−0.3178	−0.3178
α_{1T}	−0.1882	−0.1904	−0.1876	−0.1868	−0.1829	−0.1817	−0.1797	−0.1637	−0.0579	−0.0579

Table 4 Iteration history of behavior constraints for case 2 (frequency and autorotation constraints imposed)

	Iteration					
	0	1	2	3	4	5
ω_{1L}	0.7290	0.7190	0.6710	0.6540	0.6210	0.6210
ω_{1F}	1.101	1.099	1.089	1.086	1.080[a]	1.080[a]
ω_{1T}	4.251	4.203	3.993	3.919	3.797	3.797
I/I_b	1.010	0.992	0.966	0.963	0.977	0.977
α_{1L}	−0.0221	−0.0227	−0.0218	−0.0213	−0.0188	−0.0188
α_{1F}	−0.3274	−0.3347	−0.3495	−0.3519	−0.3477	−0.3477
α_{1T}	−0.1882	−0.1904	−0.1876	−0.1868	−0.1840	−0.1840

[a]Active constraint.

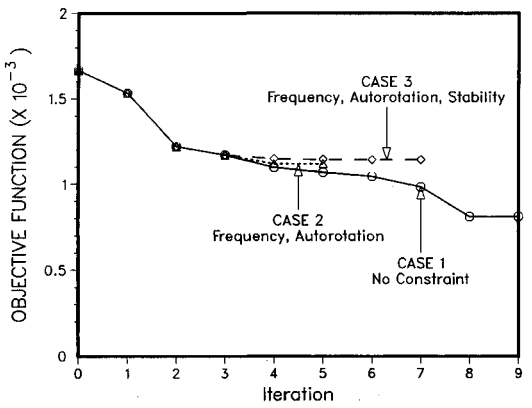

Fig. 8 Optimization iteration history of objective function for a box-beam blade.

function. When compared with the initially feasible case where no stability constraint was violated and a 77% reduction of the objective function was achieved, a much lower reduction is achieved with this initially infeasible design.

Optimization of Single-Spar Blade

The defining parameters for the baseline box-beam blade is given in Table 2. The associated fundamental rotating frequencies are 0.73/rev for the lag, 1.10/rev for the flap, and 4.25/rev for the torsion modes.

The design variables include the dimensions of the box beam (b_s,h_s,t_b,t_h) for structural parameters in addition to nonstructural design parameters (m_{ns},y_{ns}). Blade structural bending stiffnesses are obtained from the box-beam dimensions using Eq. (16). Note that a change in structural parameters of the box-beam blade influences the blade mass as well as stiffness. The side constraints for the nonstructural parameters are the same as for the generic blade case. The structural side constraints are defined as follows.

Spar width:

$$2.50 \text{ in.} \le b_s \le 3.50 \text{ in.}$$

Spar height:

$$1.00 \text{ in.} \le h_s \le 1.27 \text{ in.}$$

Spar thicknesses:

$$0.20 \text{ in.} \le t_b, t_h \le 0.50 \text{ in.}$$

The initial nonstructural mass parameters are the same as those used for the generic blade case. That is, a 1% nonstructural mass is placed forward of the elastic axis by 5% of the chord in all five blade elements. A total of 30 design variables for five beam elements are used (y_0 is not considered). For this case, the aeroelastic stability, frequency placement, and autorotational inertia constraints are all included. The minimum allowable margin of stability constraint (ε_k) for the first flap, lag, and torsion modes is chosen as 2%. The upper and lower bounds for the frequency placement constraint are selected as follows.

Lag:

$$0.60/\text{rev} \le \omega_{1L} \le 0.80/\text{rev}$$

Flap:

$$1.08/\text{rev} \le \omega_{1F} \le 1.18/\text{rev}$$

Torsion:

$$2.50/\text{rev} \le \omega_{1T} \le 6.50/\text{rev}$$

The subscripts $1L$, $1F$, $1T$ denote first lag, first flap, and first torsion modes, respectively. For an autorotation constraint, the allowable minimum value R_A of the ratio of the blade moment inertia to the baseline is chosen as 90%.

In order to examine the influence of the behavior constraints, several optimum solutions are determined while imposing different combinations of constraints. In case 1, no behavior constraints are imposed during the optimization process. The frequency placement and autorotation constraints are imposed in case 2. Finally, case 3 includes all constraints on stability, frequency, and autorotational inertia. Figure 8 shows the iteration history of the objective function

Table 5 Iteration history of behavior constraints for case 3 (all constraints imposed)

	Iteration							
	0	1	2	3	4	5	6	7
ω_{1L}	0.7290	0.7190	0.6710	0.6540	0.6400	0.6380	0.6380	0.6370
ω_{1F}	1.101	1.099	1.089	1.086	1.083[a]	1.083	1.082	1.082
ω_{1T}	4.251	4.203	3.993	3.919	3.868	3.860	3.858	3.858
I/I_b	1.010	0.992	0.966	0.963	0.969	0.970	0.971	0.971
α_{1L}	−0.0221	−0.0227	−0.0218	−0.0213	−0.0202[a]	−0.0200[a]	−0.0200[a]	−0.0200[a]
α_{1F}	−0.3274	−0.3347	−0.3495	−0.3519	−0.3501	−0.3499	−0.3496	−0.3496
α_{1T}	−0.1882	−0.1904	−0.1876	−0.1868	−0.1854	−0.1853	−0.1851	−0.1851

[a]Active constraint.

Table 6 Optimum 4P hub loads ($\times 10^{-3}$) for the box-beam blade

	Hub force			Hub moment		
	F_{XH}^{4P}	F_{YH}^{4P}	F_{ZH}^{4P}	M_{XH}^{4P}	M_{YH}^{4P}	M_{ZH}^{4P}
Baseline	0.7924	0.7243	0.3429	0.3371	0.3348	0.1932
Case 1	0.4823	0.4939	0.1705	0.0672	0.0680	0.0207
Case 2	0.6152	0.6457	0.2383	0.1312	0.1318	0.0585
Case 3	0.6187	0.6488	0.2500	0.1414	0.1419	0.0636

for these three cases. The objective function is defined in the same manner as for the generic blade case (i.e., the minimization of the 4/rev resultant due to all hub forces and moments). For case 1, a 51% reduction in the objective function is achieved relative to the initial value. For constrained optimizations, the objective function is reduced by 33% for case 2 and by 32% for case 3.

Examination of the optimization iteration history of the behavior parameters helps one to better understand the constrained optimization problems. For case 1, the values of the behavior parameters at each iteration are given in Table 3, though no behavior constraints are imposed. The fundamental rotating frequencies are continuously reduced, and the final solution represents a softer blade in bending and torsion. The flap frequency constraint would be violated after the fourth iteration if the frequency constraint were imposed. The autorotation parameter does not change significantly and would never have been violated if the minimum value R_A of 90% had been imposed. For stability, a negative value of α_k implies a positive damping of the kth mode. The lag mode damping is reduced at each iteration, and the lag mode stability constraint would be violated after the fourth iteration if the 2% minimum margin (ε_k) were imposed. The flap mode damping is reduced at each iteration, and the lag mode stability constraint would be violated after the fourth iteration if the 2% minimum margin (ε_k) were imposed. The flap mode damping is less sensitive during the iterations. The torsion mode damping is changed abruptly after the seventh iteration. This is caused by the placement of nonstructural mass aft of the elastic axis (toward the trailing edge) to achieve a significant additional reduction in the objective function. Note that a large aft shift of blade center of gravity may lead to torsion mode instability.

Table 4 shows the iteration history of the behavior parameters for case 2, where the frequency and autorotation constraints are imposed during the optimization process. As expected, the flap mode frequency becomes violated during the fourth iteration; therefore, the optimizer enforces the violated design solution to move along the feasible direction to maintain a feasible design with respect to the first flap mode frequency. As a result, the optimum solution is determined by the lower bound on the flap frequency constraint. It may be noted that the optimum blade tends to have a softer rotating frequency in all modes. For this case, the autorotation constraint never becomes active. The stability constraints are not imposed, therefore, they are not considered active even though the lag mode damping falls slightly below 2% after the fourth iteration.

For case 3, the iteration history of the behavior parameters is shown in Table 5. During optimization, the frequency, autorotation, and stability constraints are all imposed. After the fourth iteration, the flap frequency and lag mode stability constraints become active and the optimizer alters the design sequence to maintain feasibility. In subsequent iterations, the lag mode damping alone becomes active and the flap frequency stays in the feasible design space. The flap and torsion mode dampings are almost unchanged during the iterations. The autorotation constraint does not show a significant sensitivity and is never violated during the optimization iterations. In Table 6, the optimum values of 4/rev hub loads for the box-beam blade are shown. Since the objective function includes all six components of 4/rev hub forces and moments, all the components are simultaneously reduced from the baseline values. For case 1, there is a 40–90% reduction of 4/rev hub loads, compared to the baseline values. For cases 2 and 3, a 10–70% reduction of 4/rev hub loads is achieved.

Conclusions

Structural optimization is carried out on a four-bladed, soft in-plane hingeless rotor to minimize six components of oscillatory hub loads in forward flight while satisfying certain behavior constraints. Based on the results of the study, the following conclusions are made:

1) The use of a direct analytical approach for the sensitivity analysis resulted in an 80% reduction in total CPU time for optimizing the generic blade design, compared with the required CPU estimates for commonly used finite-difference approaches.

2) For a generic blade representation, an optimized design resulted in substantial reductions in oscillatory hub loads, including 60–90% reductions in all six components. Gains become smaller if an initially infeasible design is pursued. For example, if a behavior constraint of 1% lag mode damping is enforced, the objective function is reduced by 25% for the optimized solution instead of the 77% achieved with no active constraint. For a box-beam blade representation, there is a 10–90% reduction of 4/rev hub forces and moments from the baseline values.

3) The sensitivity derivatives for a blade with a spar were easily obtained by applying a simple chain rule differentiation to the formulation of the sensitivity analysis for the generic blade. The potential of the direct analytical approach was demonstrated by showing its application to a more detailed blade configuration.

4) Among behavior constraints, the frequency placement and stability constraints significantly influenced the optimum solution. For the box-beam blade, a 33% reduction of the objective function was achieved when the flap frequency constraint became active, a 32% reduction was obtained when the lag mode stability and flap frequency constraints became active, and the objective function was reduced by 51% from the baseline value when no behavior constraint was imposed.

5) The autorotation constraint was not important in determining the optimum solution for vibration reduction in the examples considered.

6) All the optimum blade designs for the hingeless rotor representations considered had softer structural stiffness in flap, lag, and torsion.

Acknowledgments

This work was supported by NASA Langley Research Center under NASA Grant NAG-1-739; technical monitor was Joanne Walsh.

References

[1]Ashley, H., "On Making Things the Best—Aeronautical Uses of Optimization," *Journal of Aircraft*, Vol. 19, No. 1, 1982, pp. 5–28.

[2]Friedmann, P. P., and Shanthakumaran, P., "Optimum Design of Rotor Blades for Vibration Reduction in Forward Flight," *Journal of the American Helicopter Society*, Vol. 29, No. 4, 1984, pp. 70–80.

[3]Miura, H., and Schmit, L. A., "NEWSUMT—A Fortran Program for Inequality Constrained Function Minimization," NASA CR-159070, 1979.

[4]Peters, D. A., Rossow, M. P., Korn, A., and Ko, T., "Design of Helicopter Rotor Blades for Optimum Dynamic Characteristics," *Computers & Mathematics with Applications*, Vol. 12A, No. 1, 1986, pp. 85–109.

[5]Vanderplaats, G. N., "CONMIN—A Fortran Program for Constrained Function Minimization," NASA TM-X-62282, 1973.

[6]Bennett, R. L., "Application of Optimization Methods to Rotor Design Problems," *Vertica*, Vol. 7, No. 3, 1983, pp. 201–208.

[7]Root, R. R., and Ragsdell, K. M., *BIAS: A Nonlinear Programming Code in Fortran IV—User's Manual*, Purdue Univ., West Lafayette, IN, 1976.

[8]Davis, M. W., and Weller, W. H., "Applications of Design Optimization Techniques to Rotor Dynamics Problems," *Journal of the American Helicopter Society*, Vol. 33, July, 1988, pp. 42–50.

[9]Vanderplaats, G. N., Sugimoto, H., and Sprague, C. M., "ADS-1: A New General Purpose Optimization Program," *AIAA Journal*, Vol. 22, No. 10, 1984, pp. 1458–1459.

[10]Lim, J. W., and Chopra, I., "Design Sensitivity Analysis for Aeroelastic Optimization of a Helicopter Rotor," *AIAA Journal*, Vol. 28, No. 1, 1990, pp. 75–82.

[11]Lim, J. W., and Chopra, I., "Stability Sensitivity Analysis for Aeroelastic Optimization of a Helicopter Rotor," *AIAA Journal*, Vol. 28, No. 3, 1990, pp. 1089–1097.

[12]Lim, J. W., and Chopra, I., "Aeroelastic Optimization of a Helicopter Rotor," *Journal of American Helicopter Society*, Vol. 34, No. 1, 1989, pp. 52–62.

[13]Celi, R., and Friedmann, P. P., "Structural Optimization with Aeroelastic Constraints of Rotor Blades with Straight and Swept Tips," AIAA Paper 88-2297, April 1988.

[14]Vanderplaats, G. N., "Approximation Concepts for Numerical Airfoil Optimization," NASA TP-1370, March 1979.

[15]Chattopadhyay, A., and Walsh, J., "Minimum Weight Design of Rectangular and Tapered Helicopter Rotor Blades with Frequency Constraints," 29th AIAA SDM Conference, Williamsburg, VA, April 1988.

[16]Miura, H., "Application of Numerical Optimization Method to Helicopter Design Problems: A Survey," NASA TM-86010, Oct. 1984.

[17]Pritchard, J. I., and Adelman, H. M., "Optimal Placement of Tuning Masses for Vibration Reduction in Helicopter Rotor Blades," 29th AIAA SDM Conference, Williamsburg, VA, April 1988.

[18]Nelson, R. B., "Simplified Calculation of Eigenvector Derivatives," *AIAA Journal*, Vol. 14, 1976, pp. 1201–1205.

[19]Panda, B., and Chopra, I., "Dynamics of Composite Rotor Blades in Forward Flight," *Vertica*, Vol. 11, No. 1, 1987, pp. 187–209.

[20]Lim, J. W., "Aeroelastic Optimization of a Helicopter," Ph.D. Dissertation, Department of Aerospace Engineering, University of Maryland, College Park, MD, May 1988.

[21]Bir, G. S., and Chopra, I., "Gust Response of Hingeless Rotors," *Journal of the American Helicopter Society*, Vol. 31, No. 2, 1986, pp. 33–46.

[22]Timoshenko, S., and Goodier, J. N., *Theory of Elasticity*, McGraw-Hill, New York, 1951.